Progress In Electromagnetics Research C, Vol. 80, 1–12, 2018

An Optimization-Based Design Technique for Multi-Band Power Amplifiers

Eyad Arabi*, Peter Bagot, Souheil Bensmida, Kevin Morris, and Mark Beach

Abstract—Matching networks for dual-band power amplifiers typically rely on complex, non-general techniques, which either use switches or result in large and lossy matching networks. In this work, mathematical optimization is employed to design the matching networks for multi-band power amplifiers. The theory of continuous modes is utilized together with accurate models for the device package to define the required impedance terminations theoretically thus allowing mathematical optimization to be used for the design. This technique depends on neither the network architecture nor the number of frequency bands. Therefore, simple and compact multi-band matching networks can be achieved. As proof of concept, a triple-band amplifier at 0.8, 1.8, and 2.4 GHz has been designed using the proposed method. The fabricated amplifier demonstrates maximum power added efficiencies of 70%, 60%, and 58% and output powers of 40 dBm, 41 dBm and 40 dBm for the three frequency bands, respectively. The presented design approach is highly suitable for the next generation of wireless systems.

1. INTRODUCTION

The evolution in wireless communications is ever growing with more users and heavier applications being introduced. As a consequence, future standards, such as the fifth generation (5G), require incredibly high data rates beyond the capacity of the frequency spectrum currently in use (below 6 GHz). Migrating to higher frequencies (mm-wave) is a costly and time-consuming process, which will take many years to unfold. Meanwhile, the sub-6 GHz bands need to be fully utilized by operating at multiple, non-adjacent bands to fulfill the immediate needs of the markets. Moreover, modern wireless systems need to operate a wide range of services such as mobile data, WiFi, GPS, etc.. To address these challenges, a multi-band system can be utilized.

In the design of multi-band wireless systems, the most challenging part is the RF front end. This work focuses on the design of the power amplifier (PA), which is one of the critical components of the RF front end. To design PAs for the applications mentioned above the optimal solution will be an ultra-wide-band design. However, if the separation between the frequency bands is large, it becomes very challenging to maintain the performance of the wide-band amplifier, and a multi-band design can be used instead.

The most critical phase in the design of multi-band PAs is typically the input/output matching networks (MNs). Multiple MNs interconnected with switches [1], tunable capacitors [2], or coupled with lumped or distributed frequency-selective resonators can be used [3]. Also, networks consist of multiple cells, which are designed recursively have been reported [4, 5]. Even though such circuits are easy to design and implement, their sizes and losses scale with the number of bands. A single MN optimized for multiple frequencies can be used to reduce the size and complexity. Designs targeting different classes of operation at different frequency bands [6], or utilizing the continuous modes [7, 8] have been reported

Received 6 September 2017, Accepted 18 October 2017, Scheduled 27 November 2017

* Corresponding author: Eyad Arabi (eyad.arabi@brisol.ac.uk).

The authors are with the Communications Systems and Networks Research Group (CSN), Department of Electrical & Electronic Engineering, The University of Bristol, Bristol, UK.

using a single MN. These works, however, use complex methods to design the MNs, which are limited to specific amplifier modes of operation and specific network topologies. Also, these design techniques do not allow the number of frequency bands to be extended above two.

In this work, a novel method for the design of single MNs for multi-band operation is presented. The continuous modes theory and mathematical optimization are combined for the first time to provide a powerful and scalable design approach. The proposed method does not require a particular MN topology and can be used with any continuous mode class of operation. Moreover, the method is based on theoretical analysis and does not rely on the costly and time-consuming load pull simulations or measurements. As proof of concept, a triple-band PA is presented with excellent agreement between the measurements and the simulations, which verifies the design method. This work extends our previous brief [9], in which the amplifier's results have been presented. In this work, the optimization method is described for the first time in Section 2.3 with extended measurements. Also, a general MN topology is proposed with a methodology to determine the order of the network (Section 2.2).

2. DESIGN METHODOLOGY

A typical PA schematic is illustrated in Fig. 1(a), where a Gallium Nitride (GaN) field effect transistor (FET) is used. For packaged transistors (as opposed to bare die transistors), it is important to differentiate between two impedance planes: the generator-plane (also known as the intrinsic-plane), and the package-plane. The generator-plane is the non-accessible plane of the solid-state device before all parasitics. At this plane, the transistor can be modeled as an ideal current generator. The package plane, on the other hand, is the accessible plane at the packaged transistor. Between the package plane and the generator-plane, there are several device parasitics and package parasitics. For GaN transistors, the device parasitics can be approximated as the capacitance between the drain and the source (C_{ds}). If the S-parameters of the package parasitics are known, the reflection coefficient at the generator-plane (Γ_{gen}) can be expressed as:

$$\Gamma_{gen} = \frac{S_{11} + \Gamma_{pkg}\left(S_{12}S_{21} - S_{11}S_{22}\right)}{1 - S_{22}\Gamma_{pkg}}, \tag{1}$$

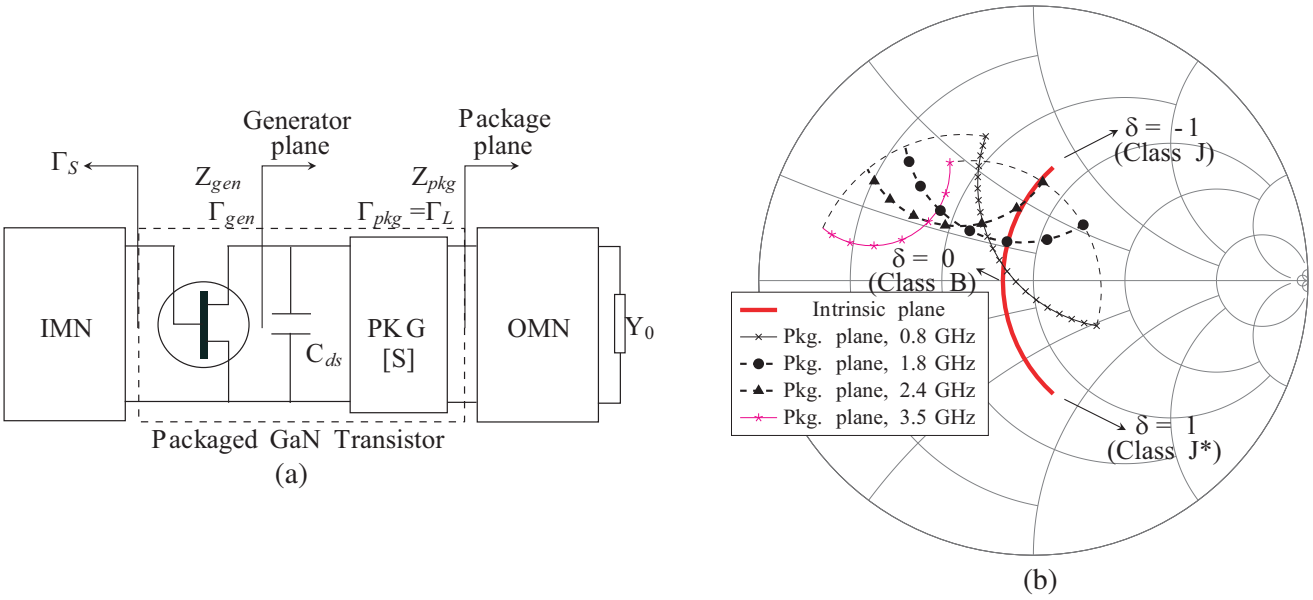

Figure 1. (a) Schematic of a typical amplifier components. (b) Design space of continuous class BV at the generator plane (frequency independent), and at the package-plane for four different frequencies. Only the terminations at the fundamental frequencies are given.

where Γ_{pkg} is the reflection coefficient at the package-plane, and S_{ij} are the S-parameters of the parasitics of the package (with C_{ds} included). If the S-parameters of the package and C_{ds} are estimated, the design of the PA can be divided into three steps as follows:

(i) Define the desired input and output impedances at all frequency bands.

(ii) Select suitable input and output MNs.

(iii) Optimize the MNs selected in step ii against the desired values defined in step i.

These steps are discussed in the following sections, respectively.

2.1. Definition of Input and Output Impedances: Continuous Class BV Theory

At the beginning of the design, the optimal source and load reflection coefficients (Γ_S and Γ_L) are determined. Γ_L is more crucial to the performance of the amplifier as compared to Γ_S; therefore, more attention is given to the output matching network (OMN). Moreover, for the case of the OMN, Γ_L is evaluated at the fundamental frequency and all its harmonics. However, the impact of Γ_L on the performance of the PA is highest at the fundamental frequency and decreases considerably as the harmonics index is increased. Therefore, in this work, only the fundamental and the second harmonic are considered.

The optimal values of Γ_S and Γ_L can be determined from load pull analysis, which provides empirical data. The other alternative is the continuous modes method first introduced by Cripps [10] for class B amplifiers. In a conventional class B PA, the transistor is biased with zero quiescent, and the output MN provide the optimal impedance at the fundamental frequency and a short circuit at all the harmonics [11]. In such case, the well-known maximum efficiency of $\Pi/4$ or 78.5% can be achieved. It has been shown in [10] that the characteristics (linearity and efficiency) of the class B amplifier can be maintained over a wider impedance space, which is known as continuous class BV or class BJ. Subsequent works demonstrate the concept of continuous modes for other classes of operation [12]. In the case of class BV, the optimal impedance at the fundamental frequency falls within an arc, which can be defined theoretically at the generator-plane. Any impedance on this arc can provide the performance of class B if the harmonics are terminated correctly. The reflection coefficients at the generator-plane for the continuous class BV at the fundamental and second harmonic are given by [10]:

$$\Gamma_{BV,1} = \frac{Z_{f_0} - Z_0}{Z_{f_0} + Z_0}, \tag{2a}$$

and

$$\Gamma_{BV,2} = \frac{Z_{2f_0} - Z_0}{Z_{2f_0} + Z_0}, \tag{2b}$$

respectively, where

$$Z_{f_0} = R_{opt}\left(1 - j\delta\right), \tag{2c}$$

$$Z_{2f_0} = j\delta\frac{3\pi}{8}R_{opt}, \tag{2d}$$

and

$$R_{opt} = 2V_{DS}/I_{\max}. \tag{2e}$$

R_{opt} is the optimal resistance at the generator-plane, which allows peak voltage swing at maximum output current. V_{DS} is the peak drain voltage and $I_{\max}$ is the maximum drain current. δ is the design space parameter, which can take any real number between -1 and 1. The design space defined in (2a) is plotted in Fig. 1(b) at both the generator and package planes, and for different frequencies.

The continuous class BV described in the previous paragraph has two distinct advantages over load-pulls: Firstly, if R_{opt}, C_{ds}, and the package parameters are estimated, it provides closed-form formulas for the optimal terminations at either the generator or the package planes as defined in Eq. (2a). Secondly, Eq. (2a) defines a design space rather than a single point. These advantages are utilized in this work to optimize the OMNs. Since the optimal terminations are theoretically defined, mathematical optimization tools can be used to optimize the OMN. Moreover, since the optimal terminations are given as a design space, they provide a broad range of objectives for the optimization routine increasing the probability of finding a solution.

2.2. Selection of the Matching Network Topology

If a particular MN architecture is selected, the algorithm presented in the next section can be used to optimize the dimensions of this architecture such that the load (Y_0) is matched to the design space defined in the previous paragraph at multiple frequencies. Selecting the right architecture or topology is key to the success of the optimization process as not all topologies are capable of solving the problem at hand. If each frequency is considered independently, the topology that provides the largest number of independent solutions for each frequency has the best chance of producing a simultaneous solution at all frequencies. If the general network of Fig. 2(a) is considered, the number of independent solutions increases as N increases; therefore, increasing N would increase the probability of producing a simultaneous solution. This can be verified by evaluating the specific problem presented later in Section 3 for different values of N as shown in Fig. 2(b), where the optimization error decreases almost exponentially as the size is increased. Increasing N, however, increases the complexity of the MN as the number of parameters is $4 \times N$ (the electrical length and characteristic admittance of each line), which complicates the tuning of the network at the full-wave simulation environment; therefore a trade-off has to be made.

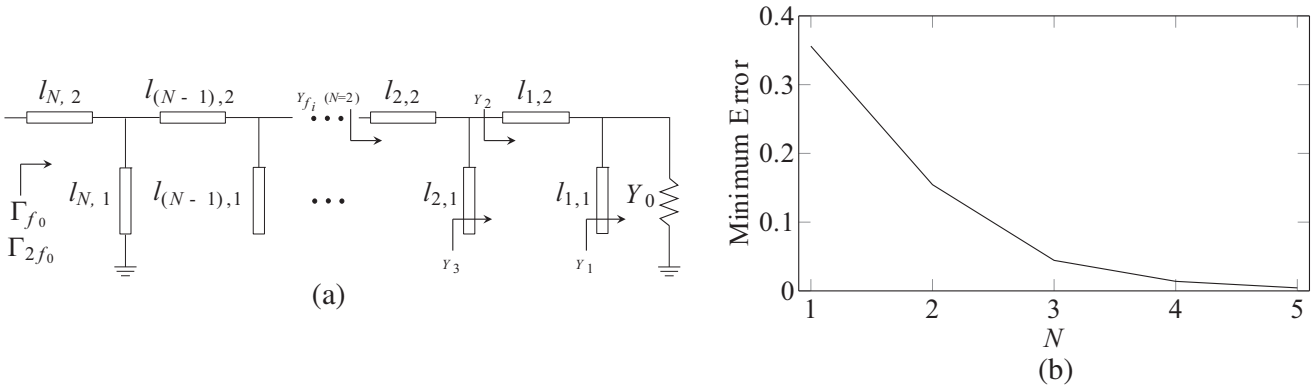

Figure 2. (a) Schematic of the general matching network used at both the input and the output of the transistor. The stub closer to the transistor is terminated with a short allowing it to be used for the DC feed. Y_1 to Y_3 and Y_{f_i} refer to the admittances defined in (8). (b) Minimum optimization error of the optimization as a function of the matching network order.

Based on the above discussion, a systematic methodology for the determination of the parameter N can be summarized as follows. Once the specific problem is defined, the optimization algorithm described in the next section can be used to produce the best solution for an increasing number of N starting from one. For each case, the performance of the amplifier is evaluated, and if the performance does not meet the requirements, N is increased by one, and the process is repeated until the required performance is achieved.

It is worth mentioning that the network presented in Fig. 2(a) has open shunt stubs except for the last stub which is terminated in a short circuit to be used as a DC feed line for the biasing of the transistor. Typically, a quarter-wave line designed for a single frequency band is used to bias the transistor. For multi-band designs complex biasing structures such as the one presented in [13, 14] can be used. For the case of the MN presented here, these complex structures are avoided because the shorted line (line N) is an integral part of the MN; therefore, it provides an inherent multi-band DC-feed line.

2.3. Optimization of the Matching Network

In this section the optimization process is described in a general form whereas a specific example is presented in the next section. The problem is defined by assigning the set of multi-band frequencies. These frequencies can be described mathematically by the following vector:

$$\overline{\mathbf{f}} = [f_1,\ f_2,\ \ldots,\ f_n]\,, \tag{3}$$

where n is the total number of frequencies. Also, the parameters of the transistor C_{ds}, R_{opt}, and the package parasitics need to be obtained from the manufacturer or estimated.

Next, the parameter N of the matching network is determined as detailed in Section 2.2. The parameters of the MN can be defined by the following vector:

$$\overline{\mathbf{D}} = [\theta_{11},\ \theta_{12},\ \ldots\ ,\theta_{N1},\ \theta_{N2}\ Z_{0,11},\ Z_{0,12},\ldots,\ Z_{0,N1},\ Z_{0,N2}] \tag{4}$$

where θ_{ij} and $Z_{0,ij}$ are the electrical lengths and characteristic impedances of the lines, respectively, and N is the order of the MN (see Fig. 2(a)).

If the parameter δ in Equation (2a) is expressed vector form as:

$$\overline{\boldsymbol{\delta}} = [-1,\ \delta_2, \delta_3, \ldots\ , \delta_{m-1},\ 1]\,, \tag{5}$$

the optimization problem can be defined mathematically as follows.

$$\min_{\overline{\mathbf{D}}} \left[\sum_{\overline{\mathbf{f}}} \min_{\overline{\boldsymbol{\delta}}} \left(\frac{w_{f_0}\overline{\Delta\Gamma}_{f_0} + w_{2f_0}\overline{\Delta\Gamma}_{2f_0}}{w_{fo} + w_{2f_0}} \right) \right], \tag{6a}$$

Subject to

$$\theta_{\min} < \theta_{ij} < \theta_{\max} \qquad i \in \{1, 2,\ \ldots\ , N\}, j \in \{1, 2\} \tag{6b}$$

$$Z_{\min} < Z_{0ij} < Z_{\max} \quad i \in \{1, 2,\ \ldots\ , N\}, j \in \{1, 2\} \tag{6c}$$

$$\theta_{12} + \theta_{22} + \ldots + \theta_{N2} < \theta_{l,\max} \tag{6d}$$

where w_{fo} and w_{2f_0} are weights assigned to increase the influence of the reflection coefficient at the fundamental frequency as compared to that at the second harmonic.

$$\overline{\Delta\Gamma}_{f_0} = \left|\overline{\Gamma}_{gen}(\overline{\mathbf{D}}) - \overline{\Gamma}_{BV,1}\right|_{\overline{\mathbf{f}}} \tag{6e}$$

and

$$\overline{\Delta\Gamma}_{2f_0} = \left|\overline{\Gamma}_{gen}(\overline{\mathbf{D}}) - \overline{\Gamma}_{BV,2}\right|_{2\times\overline{\mathbf{f}}}, \tag{6f}$$

where $\overline{\Gamma}_{gen}(\overline{\mathbf{D}})$ is an $m \times n$ matrix of the input reflection coefficients at the generator plane. To calculate $\overline{\Gamma}_{gen}(\overline{\mathbf{D}})$ the reflection coefficients at the package plane are first calculated as:

$$\overline{\Gamma}_{pkg}(\overline{\mathbf{D}}) = \begin{bmatrix} \Gamma'_{f_1}(\overline{\mathbf{D}}) & \Gamma'_{f_2}(\overline{\mathbf{D}}) & \ldots & \Gamma'_{f_n}(\overline{\mathbf{D}}) \\ \Gamma'_{f_1}(\overline{\mathbf{D}}) & \Gamma'_{f_2}(\overline{\mathbf{D}}) & \ldots & \Gamma'_{f_n}(\overline{\mathbf{D}}) \\ \vdots & \vdots & \ddots & \vdots \\ \Gamma'_{f_1}(\overline{\mathbf{D}}) & \Gamma'_{f_2}(\overline{\mathbf{D}}) & \ldots & \Gamma'_{f_n}(\overline{\mathbf{D}}) \end{bmatrix}, \tag{7}$$

where $\Gamma'_{f_i}(\overline{\mathbf{D}})$ can be defined for the case of a topology with N=2, without loosing generality, as (see Fig. 2(a)):

$$\Gamma'_{f_i}(\overline{\mathbf{D}}) = \frac{Y_0 - Y_{f_i}}{Y_0 + Y_{f_i}}, \qquad \text{and} \quad f_i \in \overline{\mathbf{f}}, \tag{8a}$$

where

$$Y_{f_i} = Y_{22}\frac{Y_{3i} + jY_{22}\tan(\theta_{22}f_i/f_1)}{Y_{22} + jY_{3i}\tan(\theta_{22}f_i/f_1)}, \tag{8b}$$

$$Y_{3i} = Y_{2i} - jY_{21}\cot(\theta_{21}f_i/f_1), \tag{8c}$$

$$Y_{2i} = Y_{12}\frac{Y_{1i} + jY_{12}\tan(\theta_{12}f_i/f_1)}{Y_{12} + jY_{1i}\tan(\theta_{12}f_i/f_1)}, \tag{8d}$$

and

$$Y_{1i} = Y_0 + jY_{11}\tan\left(\theta_{11}f_i/f_1\right). \tag{8e}$$

θ_{ij} and Y_{ij} are the electrical lengths and characteristic admittances of the transmission lines as illustrated in Fig. 2(a). The reflection coefficient at the generator plane ($\overline{\Gamma}_{gen}(\overline{\mathbf{D}})$) can be calculated from $\overline{\Gamma}_{pkg}(\overline{\mathbf{D}})$ using Eq. (1).

$\overline{\Gamma}_{BV,i}$ is also an $m \times n$ matrix for the theoretical class BV reflection coefficients calculated using Eq. (2a) and can be defined as:

$$\overline{\Gamma}_{BV,i} = \begin{bmatrix} \Gamma_{BVi,\delta_1} & \Gamma_{BVi,\delta_1} & \dots & \Gamma_{BVi,\delta_1} \\ \Gamma_{BVi,\delta_2} & \Gamma_{BVi,\delta_2} & \dots & \Gamma_{BVi,\delta_2} \\ \vdots & \vdots & \ddots & \vdots \\ \Gamma_{BVi,\delta_m} & \Gamma_{BVi,\delta_m} & \dots & \Gamma_{BVi,\delta_m} \end{bmatrix}, \tag{9}$$

where $i \in \{1, 2\}$ ($i = 1$ for the fundamental frequency and $i = 2$ for the second harmonic) and Γ_{BVi,δ_j} is the reflection coefficient calculated from Equation (2a) for a value of $\delta = \delta_j$.

The constraints of the optimization are defined in Eqs. (6b)–(6d). The first and second constraints are set to guarantee physically realizable lengths and widths of the transmission lines, respectively. In the third constraint, θ_{i2} are the electrical lengths of the series transmission lines $l_{i,2}$ (see Fig. 2(a)), and $\theta_{l,\max}$ is the maximum allowable length of the MN. This constraint is set to reduce the losses (conductor and substrate) and size by limiting the total length of the MN.

The quantity between the square brackets in Equation (6a) is the objective of the optimization, which is required to be minimized. To calculate the objective the deviations between the theoretical reflection coefficients ($\overline{\Gamma}_{BV,i}$) and the calculated reflection coefficients ($\overline{\Gamma}_{gen}(\overline{\mathbf{D}})$) are first evaluated at the fundamentals and second harmonics. Next, a weighting average between the fundamentals and the second harmonics is performed. In this step higher weights can be assigned to the fundamental to give it higher influence over the evaluated error. The weighting average, which is the quantity in brackets in Equation (6a), is an $m \times n$ matrix with m represents the variation of δ whereas n represents the variation of the frequency. Finally, the minimum values of each column are identified then added to produce a scalar quantity, which is the final objective or error of the optimization.

The optimization is also illustrated by the chart of Fig. 3(a) and explained further by the following steps.

(i) Calculate the value of N using the guidelines of Section 2.2.

(ii) An instance of $\overline{\mathbf{D}}$ is calculated by the optimizer. The first instance may be generated randomly.

(iii) Calculate the reflection coefficients at the package-plane ($\overline{\Gamma}_{pkg}(\overline{\mathbf{D}})$) at all frequencies using Equations (7) and (8).

(iv) Transform the values generated in (iii) from the package-plane to the generator-plane using Equation (1).

(v) Repeat steps iii and iv for the second harmonic values.

(vi) Use Equations (2a), (9) and $\overline{\boldsymbol{\delta}}$ to calculate the reflection coefficients for class BV ($\overline{\Gamma}_{BV,1}$) at the generator-plane for all the values of $\overline{\boldsymbol{\delta}}$.

(vii) Repeat step (vi) for the second harmonic values ($\overline{\Gamma}_{BV,2}$) using Equation (2b).

(viii) Calculate the vectorial difference (error) between the theoretical and evaluated reflection coefficients at the fundamental frequency by subtracting the two matrices $\overline{\Gamma}_{BV,1}$ and $\overline{\Gamma}_{pkg}(\overline{\mathbf{D}})$ then evaluating the magnitude of each element.

(ix) Repeat step viii for the second harmonic using $\overline{\Gamma}_{BV,2}$ instead of $\overline{\Gamma}_{BV,1}$.

(x) Calculate the total error by weight-averaging the matrices of steps viii and ix. The weighting average is performed between each corresponding elements. Next, evaluate the total error from the resultant $m \times n$ matrix by adding the minimum elements of each column to produce a scalar quantity which is the objective of the optimization.

(xi) The error produced in step x is passed to the optimizer, which decides whether the termination criteria is met or not. If the termination criteria is met, the values of $\overline{\mathbf{D}}$ are returned and the optimization is terminated. If the termination criteria is not met, a new value of $\overline{\mathbf{D}}$ is generated and the process is repeated from step ii.

This work does not focus on the optimizer because the field of mathematical optimization is mature with many good optimizers available commercially. Therefore, the exact termination criteria and selection of the next $\overline{\mathbf{D}}$, which are handled by the optimizer, are not discussed here.

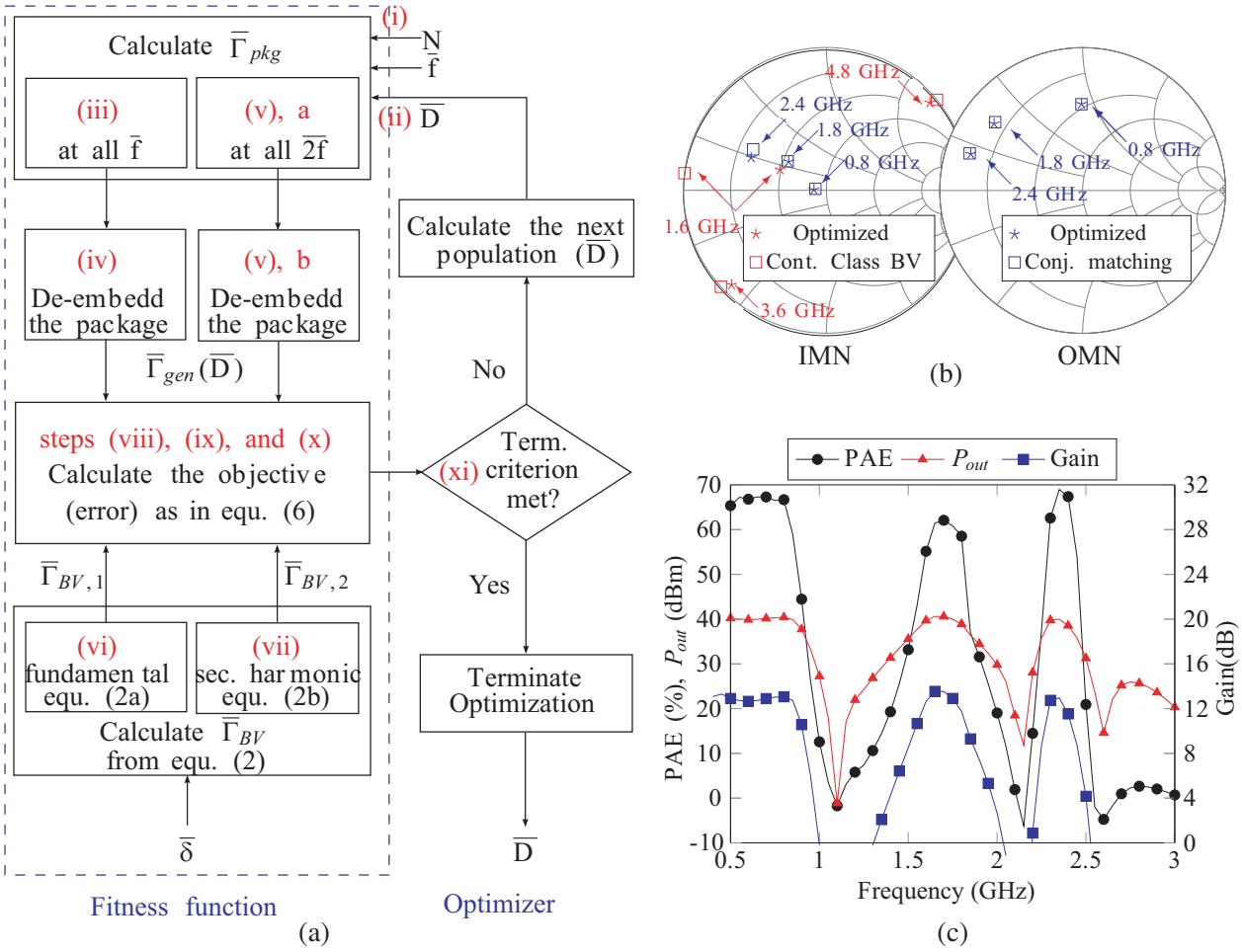

Figure 3. (a) Flowchart of the optimization algorithm. In this work, a genetic algorithm optimizer is used; however, other optimizers can also be employed. (b) Theoretical and optimized complex impedances (at the package-plane) at the fundamental frequencies as well as the second harmonics for the input matching network (IMN) and OMN. (c) Simulated PAE, P_{out}, and Gain of the triple-band PA.

3. PROOF OF CONCEPT: DESIGN OF A TRIPLE-BAND PA USING A GENETIC ALGORITHM

As proof of concept, a triple band PA at 0.8 GHz, 1.8 GHz, and 2.4 GHz has been designed. The network topology presented in Fig. 2(a) has been used for both the input and output MNs. The guidelines of Section 2.2 have been used to identify the smallest order (N) which provides the required performance. It has been found that a value of $N = 2$ produces efficiencies of around 70% for all three frequencies. In Fig. 2(b) the optimization error is plotted against N, where it can be seen that much lower errors can be achieved with $N = 4$ or 5. However, as discussed in Section 2.2, the circuit complexity in these cases increases.

The optimization of the OMN has been performed as detailed in Section 2.3. The substrate used is RT/Duroid 5880 with a dielectric constant of 2.2 and a thickness of 0.787 mm. The optimization method is independent on the particular algorithm. In this proof of concept, a genetic algorithm (GA) has been used because, unlike gradient methods, it can avoid local solutions [15].

The optimized dimensions obtained after running the GA are reported in Table 1. As expected, δ has a different value for each frequency verifying that the MN is optimized for a different class BV point at each frequency. The results of the optimization for the OMN are illustrated in Fig. 3(b) as

compared to the theoretical values of class BV. It can be observed that even though the MN used is relatively simple ($N = 2$), very accurate values have been obtained. Since the second harmonic of the low frequency is 1.6 GHz and the medium frequency (1.8 GHz) are very close, a compromise has to be made. In this example the fundamental has been assigned three-times the weight of the second harmonic ($w_{f_0} = 3$, $w_{2f_0} = 1$); therefore, the algorithm returned an impedance close to 1.8 GHz. These kinds of compromises are inevitable when the harmonics of the lower frequencies fall close to some of the higher frequencies. The simulated and measured results presented in the following section show that the proposed algorithm can handle this scenario because of the weighting average technique.

Table 1. Optimization results. The electrical lengths are all evaluated at 0.8 GHz.

	OMN				IMN			
Line No.	$L1$	$L2$	$L3$	$L4$	$L1$	$L2$	$L3$	$L4$
θ (deg)	17	20	55	18	46.5	10.1	68.7	54.4
Z_0 (Ω)	50	44	67	34	34	48.8	78.5	75.4
freq. (GHz)	0.8		1.8		2.4			
δ	0.1758		0.0248		0.0577			

The optimization of the IMN has been performed in a similar manner with only the fundamental frequencies considered. The results of the optimization are presented in Fig. 3(b) with very accurate results achieved at all three frequencies.

Next, both the input and output matching networks have been tuned using a full wave simulator for the Duroid 5880 substrate. The initial and optimized physical dimensions are given in Table 2. The S-parameters of the full wave model have been incorporated into the circuit simulation and the resultant PAE, Gain and output power (P_{out}) are shown in Fig. 3(c). The design achieves a maximum power added efficiency (PAE) of about 68%, 62%, and 69% for the low, middle, and high bands, respectively. The slightly lower efficiencies at the low and middle bands is a direct consequence of the second harmonic of the low frequency falling near the middle frequency as shown in Fig. 3(b). It can also be observed that the efficiency and P_{out} drop significantly at 1.1 GHz, 2.15 GHz, and 2.6 GHz. The first two drops are caused by the transmission zeros of the IMN, whereas the last one is caused by the transmission zero of the OMN. Such transmission zeros are beneficial because they attenuate the out-of-band transmission.

Table 2. EM optimized dimensions compared to the initial dimensions. All dimensions are in millimetre.

	OMN				IMN			
Line No.	1	2	3	4	1	2	3	4
$W_{initial.}$	2.4	2.9	1.5	4.1	4.1	2.5	1.1	1.2
W_{EM}	2.3	2.7	1.5	4.1	3.5	1.2	0.9	3.7
$L_{init.}$	12.9	15	42.3	13.4	34.7	7.6	53.2	42.1
L_{EM}	9	14.75	39	14	42*	9.3	49.5	40.6

*Bent Line

4. IMPLEMENTATION AND MEASUREMENTS

A schematic of the complete PA design is illustrated in Fig. 4(a). A GaN, high-electron-mobility transistor (HEMT) is used (CGH40010 from CREE) and the fabricated prototype of the triple-band PA is shown in Fig. 4(b). The measured results are presented and discussed in the following sections.

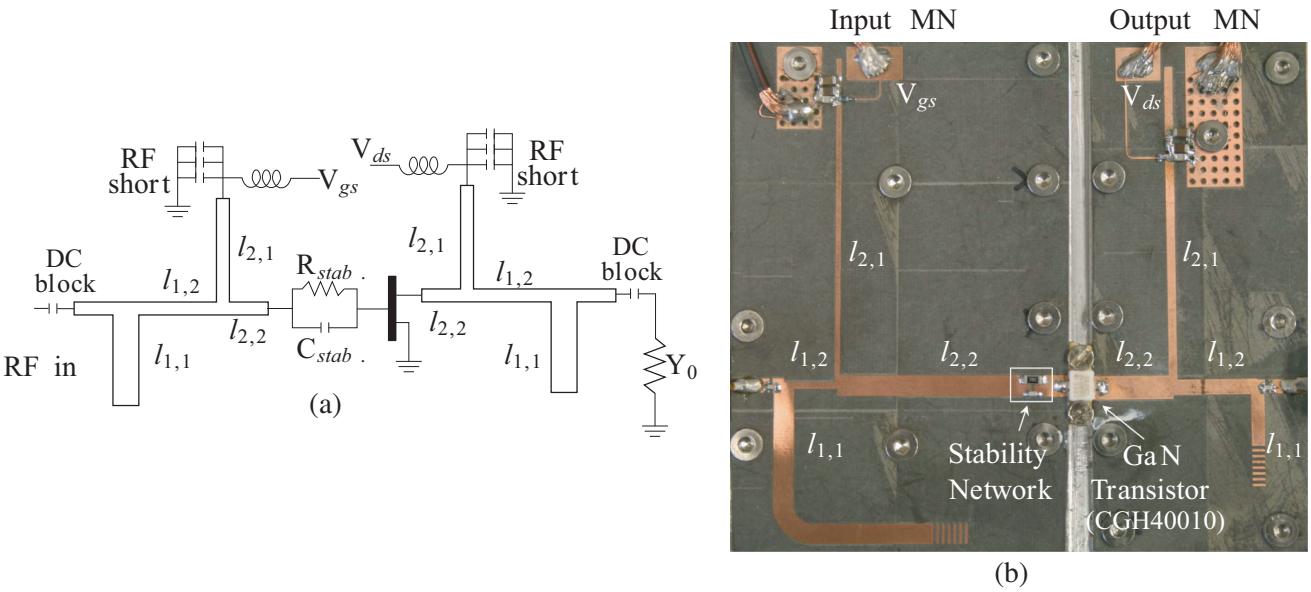

Figure 4. (a) Schematic of the triple-band amplifier. $R_{stab.}$ and $C_{stab.}$ are the resistor and capacitor of the stability network, respectively. (b) Photograph of the fabricated power amplifier.

4.1. Continuous Wave Measurements and Discussion

In the first measurements, a single tone continuous wave (CW) signal has been used with a compression point of 2 dB or less. Also, the measurements have been restricted to frequencies where the efficiency is high to maintain the temperature of the device. The measured and simulated PAEs, P_{out} and gains are plotted in Fig. 5 for the three frequency bands. A good agreement between the simulation and the measurement can be observed. For the lower band, the PA provides a maximum PAE of 70% and an output power of 40 dBm with a flat gain of about 12 dB. For the middle and high bands, the maximum PAE is 60% and 58%, respectively. The output powers for these bands are 41 dBm and 40 dBm, respectively, and the gains are about 12 dB and 11 dB, respectively. The measured PAEs at the middle and high bands are slightly lower than the simulation. This discrepancy can be attributed to the parasitics of the MNs and the fabrication tolerances, which are evident in the frequency shift

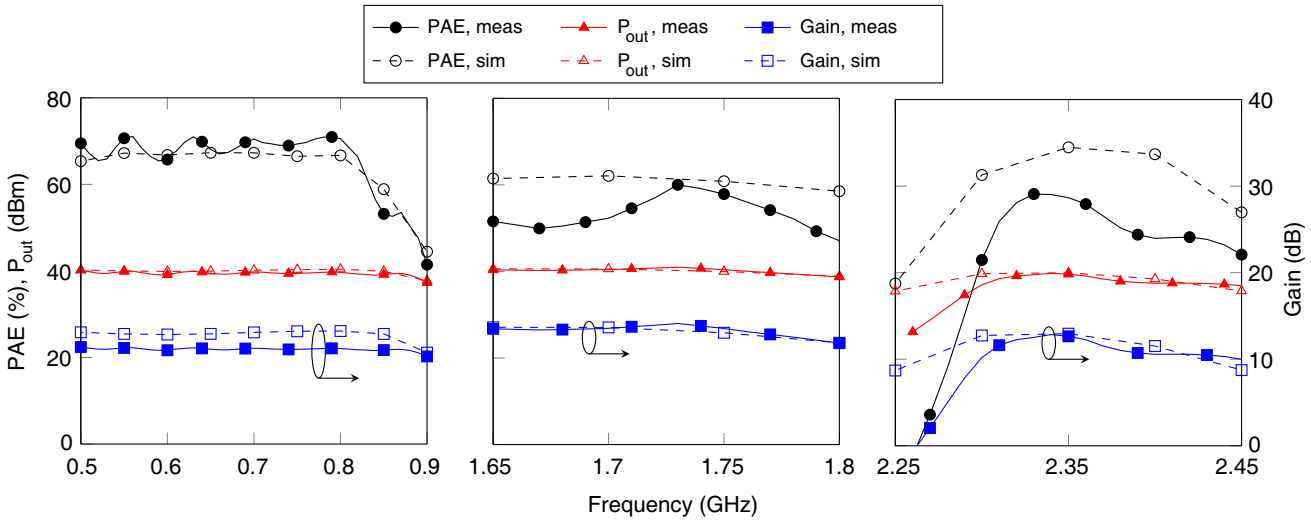

Figure 5. Simulated and measured PAE, power gain, and output power across the three frequency bands for constant input power of 27 dBm.

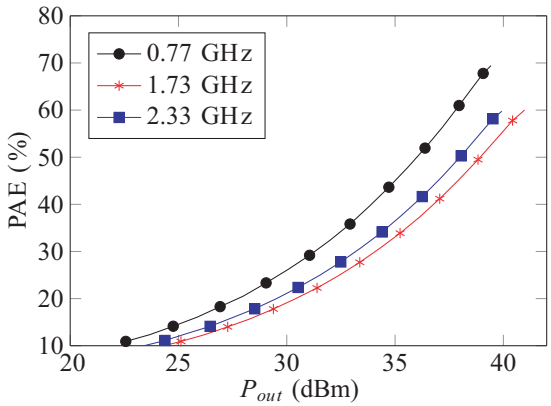

Figure 6. The measured PAE as a function of the output power for three different frequencies.

Table 3. Comparison between this work and other multi-band amplifiers.

Ref.	Frequency (GHz)	Class	P_o(dBm)	PAE_{max}%	Gain (dB)	Δf
[8]	0.8/1.9	J	$45/45^{+}$	$68/69^{+}$	$11/11^{+}$	1.1
[7]	2.15/2.25	ABJ	$45/43^{+}$	$53/59.4^{+}$	$11/11.4^{+}$	0.4
[16]	1.9/2.6	AB	$41/40^{\ddagger}$	$72/66^{\ddagger}$	$10/10^{\ddagger}$	0.7
[17]	1.7/2.6	AB	$41/41^{\ddagger}$	$70/64^{\ddagger}$	$11/11^{\ddagger}$	0.9
[1]	0.9/1.5/2	B	$29/30/30^{\dagger}$	$62/61/60^{\dagger}$	$11/10/11^{\dagger}$	1.1
[3]	0.9/1.8/2.1	AB	$30/30/31^{\dagger}$	$55/56/63^{\dagger}$	$10/11/12^{\dagger}$	1.2
[18]	1/1.5/2.5	AB	$40/41/39^{+}$	$56/58/43^{+}$	N.A.	1.5
[14]	1.49/2.15/2.65	AB	$41/41/42^{\star}$	$57/60/50^{\star}$	$11/10/10^{\star}$	1.16
This work	0.7/1.73/2.33	BJ	$40/41/40^{\star}$	$70/60/58^{\star}$	$12/12/11^{\star}$	1.83
$\star$ 2 dB compression.			† 3 dB compression.			
‡ 4 dB compression.			+ compression data not available.			

of the transmission zero at the highest frequency. Also, the exact length of line $l_{2,1}$ is affected by the manual soldering of the grounding capacitors as shown in the photo of Fig. 4(b). Nevertheless, these results verify the capabilities of the design methodology to provide good performances at three different frequencies using such a simple MN. The PAE is also plotted against the output power for all three bands as shown in Fig. 6 where very close profiles can be observed.

In Table 3, these results are compared with triple-band PAs reported in the literature. It can be observed that the presented design provides the highest frequency span (the difference between the minimum and maximum frequency bands), which is 330 MHz larger than the closest. Also, it can be observed that this design provides a high combination of gain, output power and efficiency for all three frequencies. Therefore, it can be concluded that the results of the proposed design method compare well with the results of other reported methods (even dual bands) with the added benefits of generality and scalability.

4.2. Modulated Signal Measurements and Discussions

To test the amplifier's ability to be linearized, an long term evolution (LTE) signal was used for the second measurements. The signal has a wide bandwidth of 20 MHz and a peak-to-average power-ratio (PAPR) of 8 dB. The measurement set up used was as follows. The LTE signal was generated at baseband using a modulation generator (Rohde & Schwarz AFQ 100B), the I and Q signals were fed into a vector signal generator (Keysight E8267D 250 kHz 44 GHz PSG), which provides the required RF signal. The resultant RF output of the amplifier was attenuated and connected to a signal analyzer (Rohde & Schwarz FSQ 26), where the RF signal was down-converted to the I/Q signals. These signals

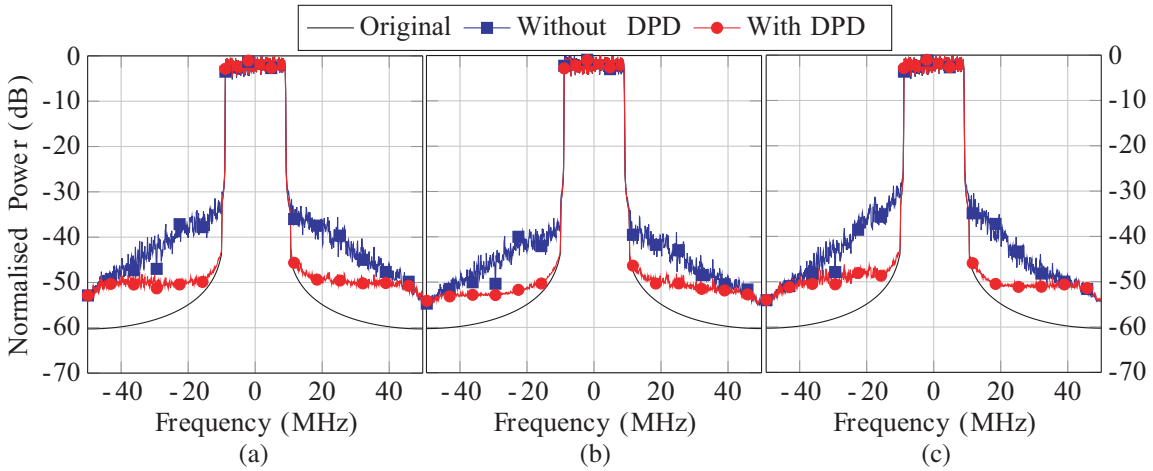

Figure 7. Response to a 20 MHz LTE signal with and without digital pre-distortion (DPD). (a) With center frequency of 0.77 GHz. (b) With center frequency of 1.77 GHz. (c) With center frequency of 2.33 GHz.

are compared to the original I/Q signal in order to calculate and apply digital pre-distortion (DPD). The pre-distorted signal was then uploaded to the baseband generator to compare the results of the DPD.

A ninth order memory polynomial with a memory depth of two has been used. Results were taken at the three operational frequencies of 0.77 GHz, 1.77 GHz, and 2.33 GHz. After the pre-distorted signal was uploaded to the baseband generator, the output signal was recaptured using the signal analyzer; Fig. 7 shows the spectrum of the PA output signal with and without DPD. The results indicate that at all three operational frequencies, by pre-distorting the LTE signal, it was possible to compensate for the PA non-linear behavior.

5. CONCLUSION

In this work, a new design methodology based on the continuous modes is presented. This design approach eliminates the need for complex and multiple MNs typically used for the design of multi-band PAs. A triple-band amplifier has been designed and tested to demonstrate the impact of the new approach. This amplifier uses MNs much simpler than the ones used for most of the reported multi-band designs with comparable PAEs. The proposed technique can be extended to design multi-band amplifiers with larger number of bands or even wideband amplifiers by positioning the optimization frequencies close together.

ACKNOWLEDGMENT

The authors would like to thank Dr. Konstantinos Mimis for his valuable comments and discussions.

This work is supported by the British Engineering and Physical Sciences Research Council (EPSRC), under the FARAD project with grant number EP/M01360X/1 in collaboration with the University of Sheffield, Sheffield, UK.

Data related to this paper is available via the University of Bristol Research Data Repository. DOI: 10.5523/bris.bc91n1n4cxjo26287i5njuq24.

REFERENCES

1. Fukuda, A., H. Okazaki, S. Narahashi, T. Hirota, and Y. Yamao, "A 900/1500/2000-MHz triple-band reconfigurable power amplifier employing RF-MEMS switches," *IEEE MTT-S International Microwave Symposium Digest 2005*, 4, Jun. 2005.

2. Sessou, K. K. and N. M. Neihart, "An integrated 700–1200-MHz class-F PA with tunable harmonic terminations in 0.13-μm CMOS," *IEEE Transactions on Microwave Theory and Techniques*, Vol. 63, 1315–1323, Apr. 2015.
3. Fukuda, A., H. Okazaki, S. Narahashi, and T. Nojima, "Concurrent multi-band power amplifier employing multi-section impedance transformer," *2011 IEEE Topical Conference on Power Amplifiers for Wireless and Radio Applications (PAWR)*, 37–40, Jan. 2011.
4. Colantonio, P., F. Giannini, R. Giofre, and L. Piazzon, "A design technique for concurrent dual-band harmonic tuned power amplifier," *IEEE Transactions on Microwave Theory and Techniques*, Vol. 56, 2545–2555, Nov. 2008.
5. Giofre, R., P. Colantonio, F. Giannini, and L. Piazzon, "A new design strategy for multi frequencies passive matching networks," *2007 European Microwave Conference*, 838–841, Oct. 2007.
6. Negra, R., A. Sadeve, S. Bensmida, and F. M. Ghannouchi, "Concurrent dual-band class-F load coupling network for applications at 1.7 and 2.14 GHz," *IEEE Transactions on Circuits and Systems II: Express Briefs*, Vol. 55, 259–263, Mar. 2008.
7. Carrubba, V., S. Maroldt, M. Muer, H. Walcher, F. Van Raay, R. Quay, O. Ambacher, D. Wiegner, U. Seyfried, T. Bohn, and A. Pascht, "Realization of a 30-W highly efficient and linear reconfigurable dual-band power amplifier using the continuous mode approach," *International Journal of Microwave and Wireless Technologies*, Vol. 6, No. 2, 115–128, 2014.
8. Fu, X., D. T. Bespalko, and S. Boumaiza, "Novel dual-band matching network for effective design of concurrent dual-band power amplifiers," *IEEE Transactions on Circuits and Systems I: Regular Papers*, Vol. 61, 293–301, Jan. 2014.
9. Arabi, E., P. D. Falco, J. Birchall, K. Morris, and M. Beach, "Design of a triple-band power amplifier using a genetic algorithm and the continuous mode method," *IEEE Radio Wireless Week*, Feb. 2017.
10. Cripps, S. C., P. J. Tasker, A. L. Clarke, J. Lees, and J. Benedikt, "On the continuity of high efficiency modes in linear RF power amplifiers," *IEEE Microwave and Wireless Components Letters*, Vol. 19, 665–667, Oct. 2009.
11. Cripps, S. C., *Advanced Techniques in RF Power Amplifier Design*, Artech House, Norwood, MA, 2002.
12. Ozen, M., R. Jos, and C. Fager, "Continuous class-E power amplifier modes," *IEEE Transactions on Circuits and Systems II: Express Briefs*, Vol. 59, 731–735, Nov. 2012.
13. Gu, L., W. Che, S. Chen, M. Zhang, Q. Cai, and Q. Xue, "Dual-band GaN power amplifiers with novel DC biasing networks incorporating offset DSPSL," *2015 IEEE MTT-S International Microwave Workshop Series on Advanced Materials and Processes for RF and THz Applications (IMWS-AMP)*, 1–4, Jul. 2015.
14. Xuan, A. N. and R. Negra, "Design of concurrent multiband biasing networks for multiband RF power amplifiers," *2012 42nd European Microwave Conference (EuMC)*, 1–4, Oct. 2012.
15. Salomon, R., "Evolutionary algorithms and gradient search: Similarities and differences," *IEEE Transactions on Evolutionary Computation*, Vol. 2, 45–55, Jul. 1998.
16. Pang, J., S. He, C. Huang, Z. Dai, C. Li, and J. Peng, "A novel design of concurrent dual-band high efficiency power amplifiers with harmonic control circuits," *IEEE Microwave and Wireless Components Letters*, Vol. 26, 137–139, Feb. 2016.
17. Chen, P., S. He, X. Wang, and Z. Dai, "1.7/2.6 GHz high-efficiency concurrent dual-band power amplifier with dual-band harmonic wave controlled transformer," *Electronics Letters*, Vol. 50, 184–185, Jan. 2014.
18. Wang, Z. and C. W. Park, "Concurrent tri-band GaN HEMT power amplifier using resonators in both input and output matching networks," *2012 IEEE 13th Annual Wireless and Microwave Technology Conference (WAMICON)*, 1–4, Apr. 2012.